UDK 621.822: 620.1/.2
Original scientific article/Izvirni znanstveni članek

ISSN 1580-2949
MTAEC9, 44(6)335(2010)

THE INFLUENCE OF POWDER SELECTION AND PROCESS CONDITIONS ON THE CHARACTERISTICS OF SOME OIL-RETAINING SINTERED BRONZE BEARINGS

VPLIV IZBIRE PRAHOV IN POGOJEV IZDELAVE NA LASTNOSTI SAMOMAZALNIH SINTRANIH LEŽAJEV VRSTE Cu-Sn

Borivoj Šuštaršič, Matjaž Godec, Aleksandra Kocijan, Črtomir Donik

Institute of Metals and Technology, Lepi pot 11, 10000 Ljubljana, Slovenia
borivoj.sustarsic@imt.si

Prejem rokopisa – received: 2010-03-23; sprejem za objavo – accepted for publication: 2010-07-26

A chemical, microstructural and mechanical characterisation of sintered bronze bearings from three different producers was performed. The investigated bearings differ considerably in their final functional properties in spite of the fact that they all have similar bulk chemical compositions and a similar basic process of their manufacture. Therefore, on the basis of the performed characterization of these bronze bearings, the reasons for their good or bad functional properties were analysed and reported.

Keywords: oil-retaining self-lubricating sintered bronze bearings, chemistry, microstructure and mechanical properties, analysis and comparison, the influence of process conditions

Kemijsko, mikrostrukturno in mehansko smo opredelili vzorce sintranih ležajev treh različnih dobaviteljev. Čeprav imajo vsi trije ležaji podobno povprečno kemijsko sestavo in naj bi bili izdelani po enaki konvencionalni sinter tehnologiji, se med seboj močno razlikujejo po svojih končnih funkcionalnih lastnostih. Zato na osnovi izvedene karakterizacije ležajev poizkušamo analizirati vzroke za dobre oz. slabše funkcionalne lastnosti posameznih ležajev.

Ključne besede: naoljeni samomazalni ležaji, kemijska, mikrostrukturna in mehanska karakterizacija, analiza in primerjava ležajev, vpliv procesnih parametrov

1 INTRODUCTION

Porous, oil-retaining bearings are both the best known and the most widely used bearing type[1]. They are usually produced by conventional sintering technology, i.e., the uniaxial automatic die compaction (ADC) of the powder mixture and sintering in a protective atmosphere. The essential element of this technology is to ensure the appropriate open porosity that is able to retain and, during hydrodynamic loading of bearing, supply of suitable oil content into the gap between the shaft and the bearing's sliding surfaces. The porosity of this type of bearings is between 15 % and 25 %, i.e., the so-called open porosity. This means that the pores are mutually interconnected. The appropriate open porosity of the bearing enables its full impregnation. The open pores are infiltrated to at least 90 %. The industrial impregnation of the bearings with oil is performed in vacuum chambers. First, the air is evacuated from the pores and then the bearings are dipped into the special oil. The average size of the pores and their size distribution mainly depend on the powder used, as well as the compaction and sintering conditions. Standard, sintered, tin-bronze bearings have the mass fraction of Sn approximately 10 %. The German standard DIN 30910, Part 3, gives the composition and the properties[2]. In sintering practice it is possible to use a powder mixture of elemental powders (Cu, Sn etc.), as well as alloyed powder with a homogeneous final chemical composition of each of the powder particles (in our case Cu-10 % Sn). In some cases, pre-alloyed powder, i.e., only a partial alloying of basic Cu particles, can also be used[1,3,4]. Generally, in all cases the powder particles have an irregular shape. Atomized powders are more globular, but pure elemental Cu powder produced by electrolysis has a dendritic or needle-like shape. Cu powder can also be produced by the reduction of ground copper oxide in a continuous belt furnace with hydrogen, dissociated ammonia or an endothermic atmosphere. Low-melting-point tin powder, usually produced by air atomization, has regularly (i.e., spherically) shaped particles[5]. The selected powder, compaction pressure and sintering conditions define the final functional properties of the bearing.

Sintered, self-lubricating, oil-retaining Cu-10 % Sn bearings from three different producers were investigated and analysed in this study. The bearings exhibit a large difference in quality and functionality. The bearing designated as bearing *A*, built in motors for liquid flow regulation and the opening of valves, endures under the standard loading test conditions for more than 150 000 cycles (open/close). However, the bearings designated as *B* and *C* can cope with much fewer (less than 25 000 cycles). **Figure 1a** shows the bearing *C* after just 15 000

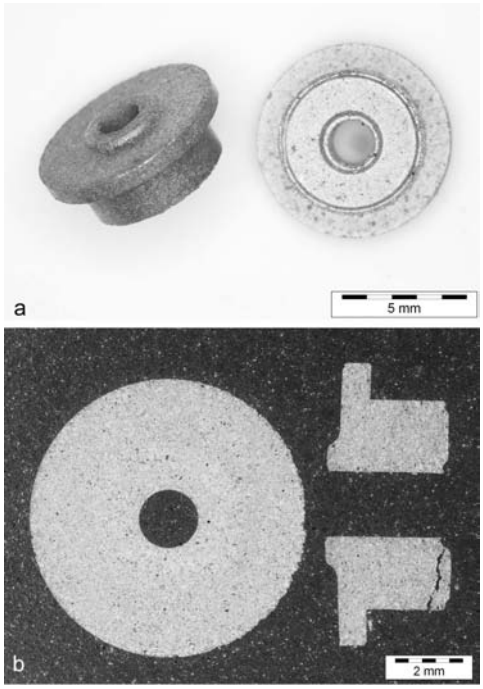

Figure 1: Snap-shot of bearing *C* (a), original magnification 6.7-times, and macro snap-shot of metallographic sample (b), Stereo microscope Olympus SZ61

Slika 1: Makroskopski posnetek ležaja *C*: (a) originalna povečava 6,7-krat in makro posnetek metalografskega obrusa pri originalni povečavi 10-krat (b); Stereo mikroskop Olympus SZ61

cycles of operation. It has been found eccentricity and visible tracks of wear debris. The reasons for such large differences in the bearings' behavior and life time were therefore established. A complete analysis and comparison of the bearings were performed. The results of the analyses, as well as the findings and possible reasons for the differences in the bearings' behavior are given below.

2 EXPERIMENTAL

The present sintered, self-lubricating bearings should be manufactured in accordance with the German standard[2] in quality Sint B-50. This declares the chemical composition (Cu with 9 % to 11 % Sn), the bearings' porosity of 20 ± 2.5 %, the sintered density from 6.8 g/cm^3 to 7.2 g/cm^3 and a hardness larger than 35 HB.

The average bulk chemical composition of the investigated bearings was determined with Ion Coupled Plasma – Atom Emission Spectroscopy (ICP-AES), Perkin Elmer 2380. The investigated bearings were delivered in the oil-impregnated condition. Therefore, the samples of the bearings were de-oiled and then dissolved in a concentrated solution of gliceregia. The formed solution was then diluted, analysed and compared with standard solutions.

The thermal removal of the oil has to be avoided because it can change the composition and properties of the bearings (oxidation, the low melting point of Sn). The standard ISO 2738[6] recommends the removal of the oil from the test pieces by solvent extraction with sequential Soxhlet Extraction. This is a very difficult and time-consuming process. For practical control purposes other methods may be used. In our case, de-oiling was performed with cyclic cooking in leach, ultrasound cleaning, drying at 105 °C and weighing of the samples.

The oil density of the sintered bearings was determined picnometrically[6] in distilled water at room temperature. The method is based on Archimedes' principal. Two bearings from each producer were measured.

The Vickers hardness, with a loading of 5 kg (HV5), of the bearings was measured, initially, as proposed by the German standard[7]. However, the indentation depth was too large and, finally, the loading was decreased to 1 kg (HV1).

For the microstructural investigations under a light (LM) and a scanning electron microscope (SEM), the samples were cut into halves and put into the bakelite in two directions with respect to the compaction direction (parallel/perpendicular; **Figure 1b**). A standard metallographic preparation (grinding and polishing) of the samples was then performed. Porosity and inclusions are observed on the polished surface, but the microstructural constituents are observed on the etched surface. In our case, an alcohol suspension of ferric chloride and hydrochloric acid (5 g $FeCl_3$+10 mL HCl+100 mL alcohol) was used as the etching agent. The porosity was analysed on metallographic samples with an automatic image-analysing system (AnalySIS-pro 3.0) built into the light microscope (Microphot FXA, Nikon with 3CCD digital camera Hitachi HV-C20A).

The local microchemical composition of the bearing samples was analyzed with X-ray Energy Dispersion Spectrometry (SEM FE JEOL JSM-6500F with EDXS Inca Energy 400). The accelerating voltage of the primary electron beam was 20 kV and an analysed volume of approximately 1 μm^3 was used for the selected analyzing conditions. The EDXS method is not suitable for a determination of the local carbon and oxygen contents. It can serve as a qualitative estimate only. It must also be warned here that incomplete removal of the oil from a sample could seriously damage the electron beam source of the SEM.

3 RESULTS AND DISCUSSION

A simple thermodynamic analysis makes it possible to estimate the expected microstructures of the bearings. In our case, computer tools for the prediction of the phase equilibrium and the experimentally determined phase diagrams were used[8–10]. The selected multi-component (Cu-Sn-Pb) and binary phase diagrams (Cu-Sn, Cu-Pb in Sn-Pb) show that in our system a substitutional solid solution of Sn in Cu can be expected. The solubility of Sn in Cu at room temperature is low. In the case of a low cooling rate, therefore, besides the FCC_A1 solid solution one can also expect Cu_3Sn and the ε phase.

Figures 2 a and b show the experimentally and theoretically calculated binary Cu-Sn phase diagrams. The latter is almost completely in accordance with the experimentally determined diagram. During the sintering of the non-homogeneous mixtures, one can also expect other hard and brittle intermetallic phases, such as Cu_6Sn_5 and similar. Lead (Pb) is practically insoluble in Cu and Sn and appears as a secondary phase. In the past, it was added as an alloying element to improve the functional properties of the bearings. Nowadays, however, it is no longer used, for ecological and health reasons.

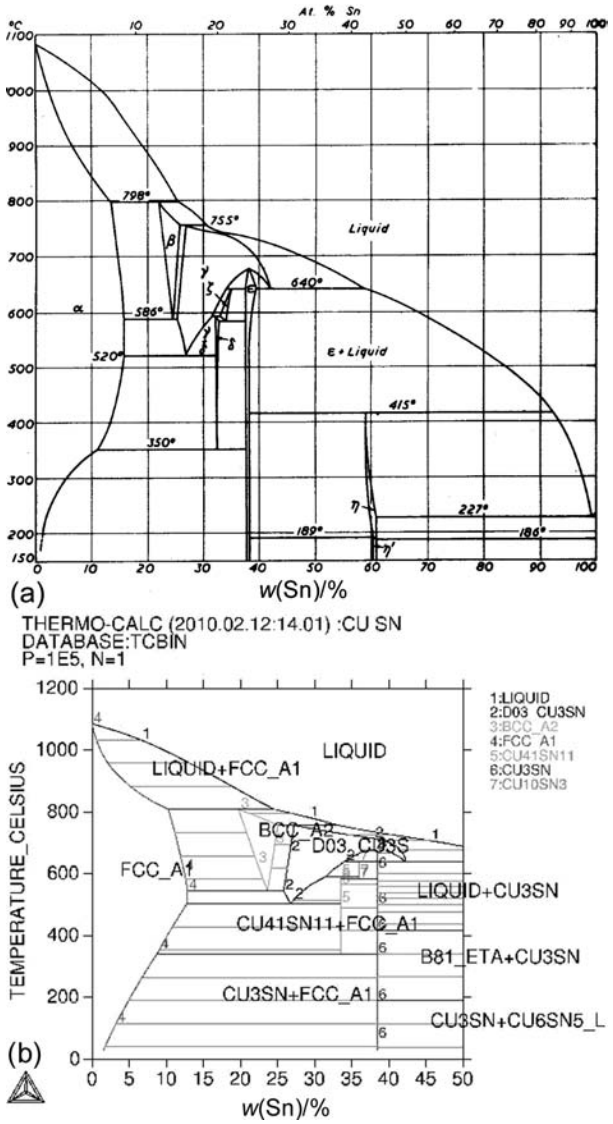

Figure 2: Equilibrium binary phase diagram of Cu-Sn with clearly visible peritectic, eutectic, eutectoid and peritectoid reactions: a) experimentally determined[9] and b) obtained with a Thermo-Calc calculation (enlarged region 0–50 % of Sn)[10]

Slika 2: Ravnotežni binarni fazni diagram Cu-Sn s peritektsko, evtektsko ter evtektoidno in peritektoidno reakcijo: a) eksperimentalno določen[9] in b) dobljen s Termo-Calc izračunom[10]; povečano območje od nič do 50 % Sn[9]

A visual inspection showed that all the investigated bearings have a golden metallic colour, typical for a bronze bearing alloy. However, they differ slightly in terms of the colour nuances, and also in terms of the design (size and shape). The average sintered densities of the oil-impregnated bearings determined with Mohr's balance are given in **Table 1**. Bearing *A* has the largest density, but bearings *B* and *C* have similar values. It is obvious that bearings *B* and *C* have a too low density, when considering DIN 30910, Part 3.

Table 1: Density of sintered bearings
Tabela 1: Gostota sintranih ležajev

Sample designation	Density (g/cm^3)	Bearing weight (g)
Bearing *A*	7.03	1.49
Bearing *B*	6.67	0.93
Bearing *C*	6.64	0.88

The results of the average bulk chemical composition of the investigated bearings are given in **Table 2**. Bearing *A* has the highest content of Sn and the lowest Pb and Zn contents. This could be a sign for the best sliding properties of this bearing. Bearings *B* and *C* have a much higher content of Pb and Zn. This means that very impure raw materials (powders) were used. The quantity of the other possible elements (As, Ni, Sb, and Al) was also checked with the ICP-AES analyzer, but the quantity of these elements was below 0.01 %.

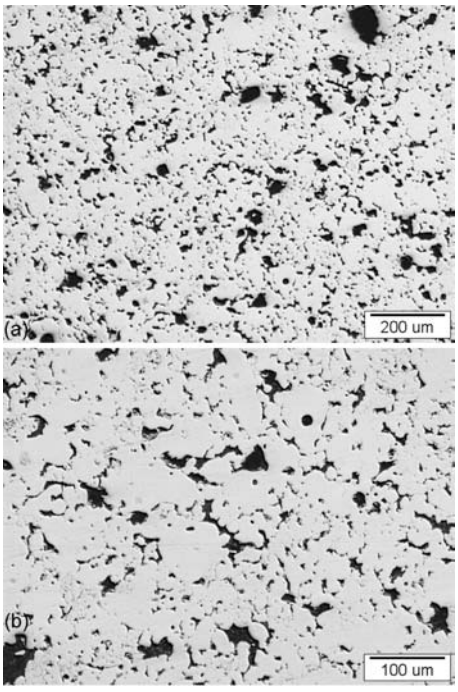

Figure 3: Microstructure of a polished sample in the middle of bearing *A*, visible at two different magnifications; direction perpendicular to ADC

Slika 3: Mikrostruktura poliranega vzorca ležaja *A* v sredini, vidna pri dveh različnih povečavah; obrus je izdelan v prečni smeri na smer stiskanja

Table 2: Average bulk chemical composition of the investigated bearings
Tabela 2: Povprečna kemijska sestava preiskovanih ležajev

Sample designation	Chemical composition (*w*/%)					Remarks
	Cu	Sn	Pb	Zn	Oil content	
Bearing *A*	88.2	10.9	0.03	< 0.005	0.62	Method of determination ICP-AES
Bearing *B*	89.8	9.5	0.07	0.09	0.58	
Bearing *C*	89.2	9.8	0.08	0.06	0.72	

Figures 3, 4 and 5 show the microstructures of polished samples of bearings *A*, *B* and *C*, with the clearly visible porosity, their shape and size distribution. Bearings *A* have typical interconnected porosity with a relatively appropriate pore size distribution. This enables good filling of the pores with oil and good sliding properties of the bearing. Larger inclusions are not present in the microstructure. Besides larger pores, mainly smaller pores are present; all located at the particle boundaries.

Larger differences in the longitudinal and perpendicular directions were not observed. Therefore, one can conclude that bearings *A* are compacted and sintered uniformly and appropriately. Bearings *B* have a much more non-uniform porosity in comparison with bearings *A*. They have a non-uniform density and porosity along the compaction direction (see **Figure 6**). The bearings are denser in thinner sections and in some regions the interconnected porosity is interrupted. The bearings *C* are very porous. A large number of very small pores are present and the already polished microstructure reveals some chemical inhomogeneity. The differences in the polished microstructure and porosity can be clearly recognized in **Figures 7 a, b and c**.

As was already mentioned, the porosity was also analysed with an automatic image-analysing system. The pore size distribution of the analysed bearings is similar (**Figures 8 and 9**), but the porosity of bearing *C* was significantly larger (approx. φ = 20 %) than those of bearings *A* and *B* (approx. φ = 10 %). **Figures 8 and 9**

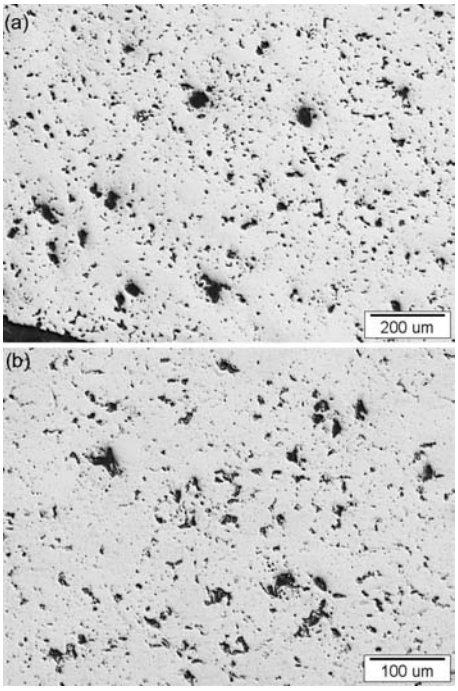

Figure 4: Microstructure of a polished sample in the middle of bearing *B*, visible at two different magnifications; direction perpendicular to ADC

Slika 4: Mikrostruktura poliranega vzorca ležaja *B*, vidna pri dveh različnih povečavah, obrus je izdelan v prečni smeri na smer stiskanja

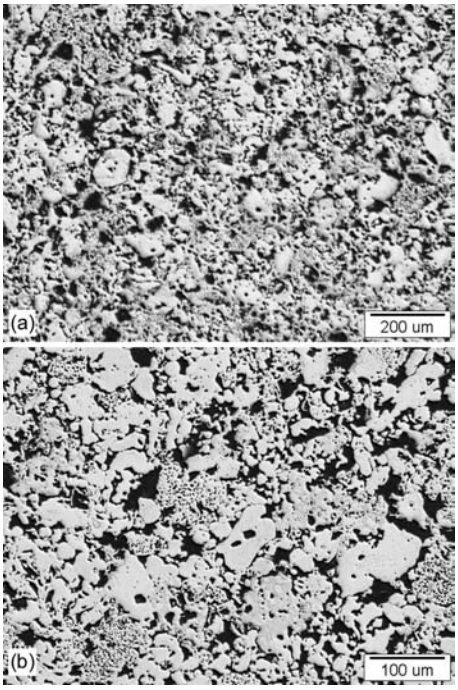

Figure 5: Microstructure of a polished sample in the middle of bearing *C* at two different magnifications; direction perpendicular to ADC

Slika 5: Mikrostruktura poliranega vzorca ležaja *C* v sredini, vidna pri dveh različnih povečavah; obrus je izdelan v prečni smeri na smer stiskanja

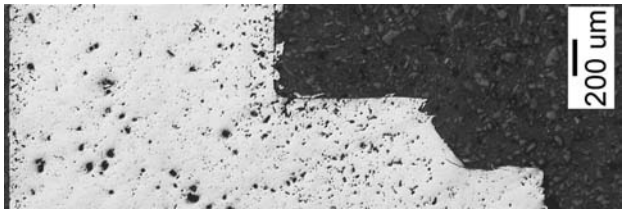

Figure 6: Microstructure of polished bearing *B* along the ADC direction, snapshot made with MIA technique

Slika 6: Mikrostruktura poliranega vzorca ležaja *B* vzdolž osi stiskanja, posnetek izdelan v MIA-tehniki

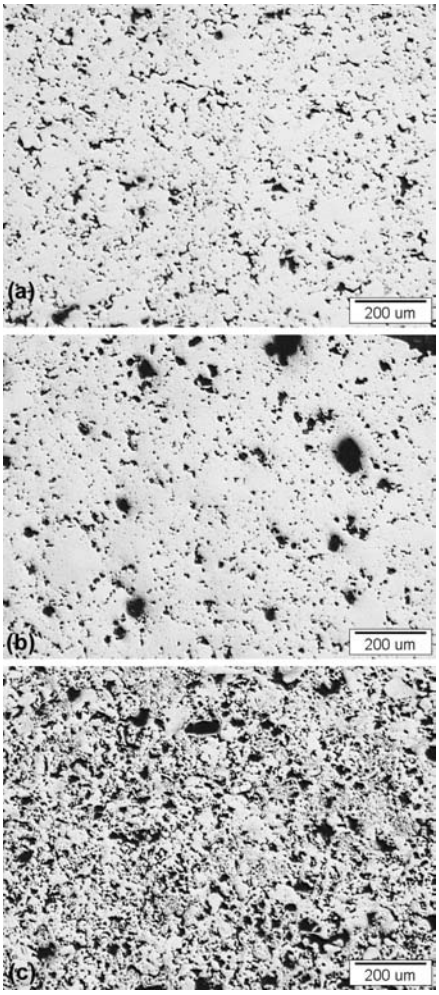

Figure 7: A comparison of microstructures of polished samples visible under LM: a) bearing *A*, b) bearing *B* and c) bearing *C*, parallel direction.

Slika 7: Primerjava med mikrostrukturami poliranih vzorcev: a) ležaj *A*, b) ležaj *B* in c) ležaj *C*, obrusi izdelani v vzdolžni smeri, sredina

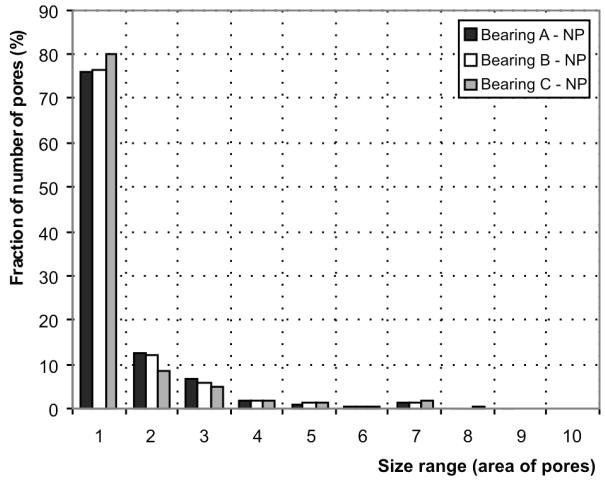

Figure 8: Histogram of pore-number distribution (NP – number of pores) inside the individual area size region.

Slika 8: Histogramski prikaz deleža števila por po posameznih velikostnih razredih (NP – število por)

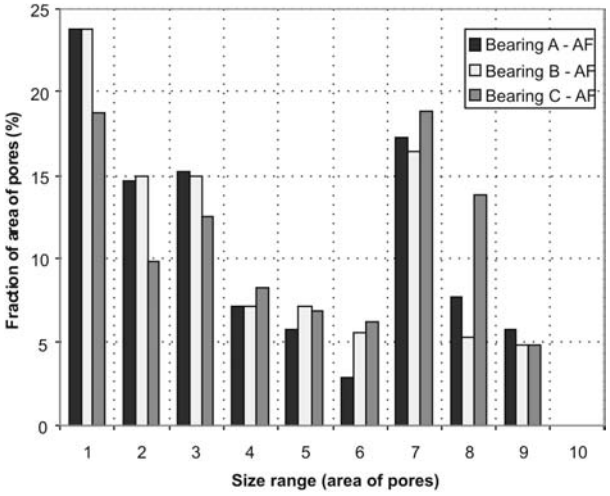

Figure 9: Histogram of the size of pore area (AF – area of pores) inside the individual area size region.

Slika 9: Histogramski prikaz ploskovnega deleža por po posameznih velikostnih razredih (AF – površina por)

show histograms of the pore number and size (area) distribution in the selected size regions (1 ≡ 0–50 μm², 2 ≡ 50–100 μm², 3 ≡ 100–200 μm², 4 ≡ 200–300 μm², 5 ≡ 300–400 μm², 6–400–500 μm², 7 ≡ 500–1000 μm², 8 ≡ 1000–2000 μm², 9 ≡ 2000–5000 μm², 10 ≡ 5000–10000 μm²). The analysis was performed at magnifications of 50, 100- and 200-times. However, only the smallest magnification gives a statistically relevant number of pores (more than 1500).

Figure 8 shows that in all three cases more than 75 % of the pores are in the smallest size range (0–50 μm²), but this represents only about 18 % to 25 % of the total volume of porosity (**Figure 9**). It is evident that bearing *C* has a larger number of the smallest pores, but a smaller number of pores in the next size regions (between 50 and 300 μm²). But, again, bearings *C* have a relatively large proportion of larger pores in the size regions between 400 μm² and 2000 μm². It should be noted here that this statistical analysis of pore number and size distribution can only serve for a qualitative assessment because it was not performed on a statistically large enough number of samples.

Figures 10, 11 and 12 show microstructures of etched samples of bearings *A*, *B* and *C*. One can observe a very nice monophase microstructure of bearing *A* (**Figure 10**), without any secondary phases present. In the microstructure, Cu twins typical for FCC structures are visible.

The Cu-Sn powder used for bearings *A* was very likely an atomized CuSn10 alloy powder with a carefully selected particle size distribution. Smaller particles fill the empty places between the larger ones. The sintering process was performed correctly with a relatively fast cooling in the final stage of the sintering. Oxide inclusions are not present. This shows an appropriately performed process with respect to the sintering

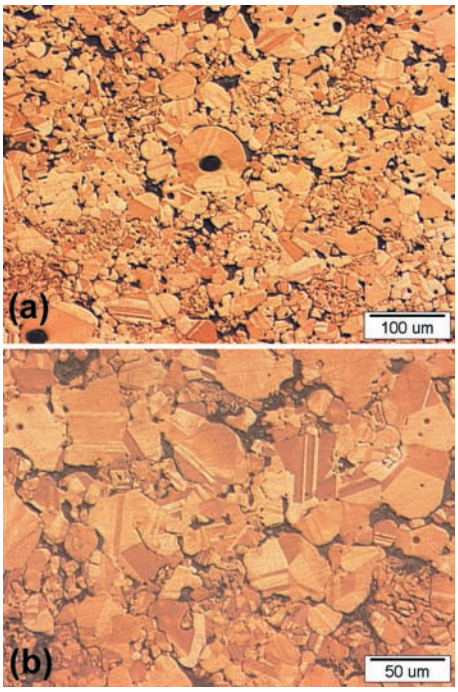

Figure 10: Microstructure of an etched sample of bearing *A*, visible at two different magnifications; perpendicular to ADC
Slika 10: Mikrostruktura zlitine jedkanega vzorca ležaja *A*:, vidna pri dveh različnih povečavah, obrus je izdelan v prečni smeri

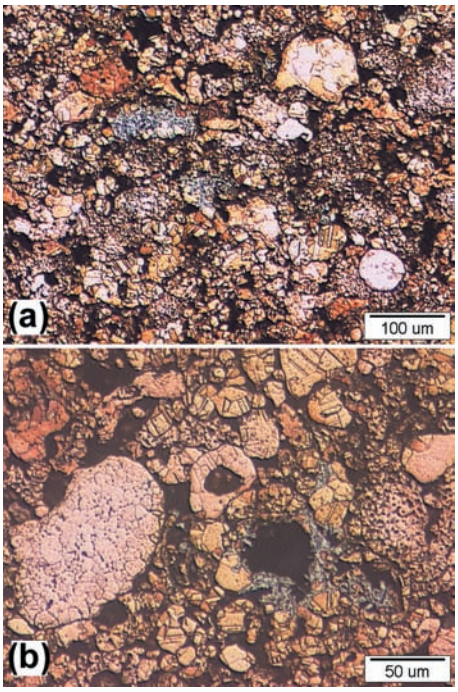

Figure 12: Microstructure of the alloy of an etched sample of bearing *C*, visible at two different magnifications; perpendicular to ADC
Slika 12: Mikrostruktura zlitine jedkanega vzorca ležaja *C*, vidna pri dveh različnih povečavah

atmosphere. Sintering the Cu89-Sn11 alloy usually runs at approx. 820 °C in a mixture of nitrogen (N_2) and hydrogen (H_2), in the ratio 70 : 30[1].

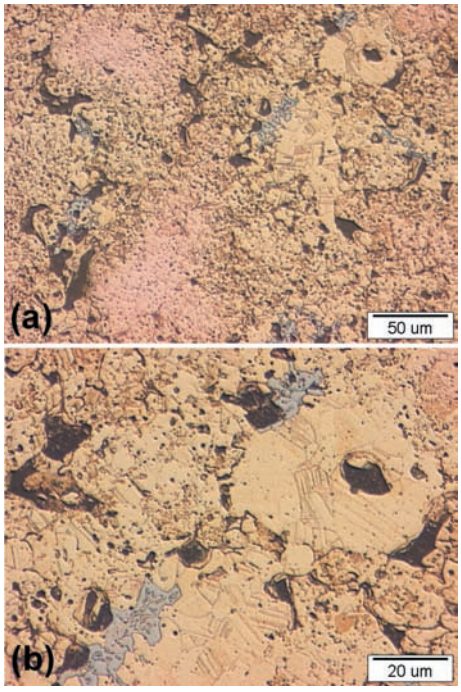

Figure 11: Microstructure of the alloy of an etched sample of bearing *B*, visible at two different magnifications; perpendicular to ADC
Slika 11: Mikrostruktura zlitine jedkanega vzorca ležaja *B*, vidna pri dveh različnih povečavah; obrus je izdelan v prečni smeri

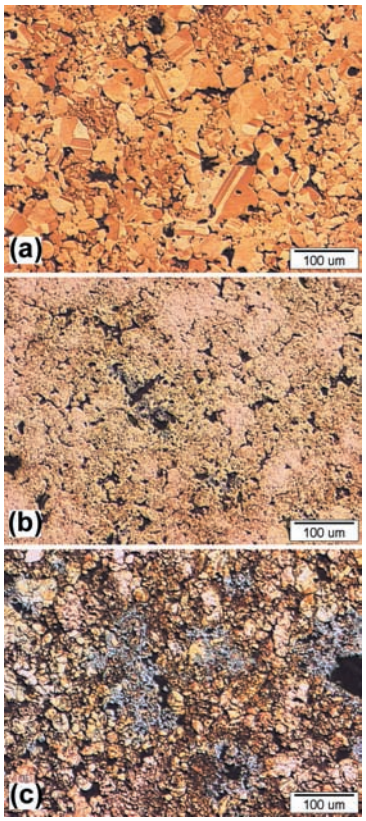

Figure 13: Comparison of the etched microstructures of alloys: a) bearing *A*, b) bearing *B* and c) bearing *C*, perpendicular to the compaction direction.
Slika 13: Primerjava med mikrostrukturami zlitin jedkanih vzorcev: a) ležaj *A*, b) ležaj *B* in c) ležaj *C*, obrusi izdelani v prečni smeri, sredina.

The microstructure of the alloy of bearing *B* (**Figure 11**) is much more heterogeneous. Larger parts of the fine pores and inclusions are present. Large fields of slightly light pink and blue show the presence of secondary phases and chemical inhomogeneity. This shows that a powder mixture consisting of elemental Cu and Sn particles was probably used.

The microstructure of bearing *C* (**Figure 12**) is also very heterogeneous. One can observe differently coloured regions. Typical FCC twins are visible here, and also regions with different chemical compositions. Inside the larger grains one can also see small subgrains. The differences in the etched microstructures of the present bearings can be easily recognized in **Figures 13 a to *c***.

In **Table 3**, the average Vickers hardness of the investigated bearings is given. Bearings *A* have the highest and the most uniform hardness values. The hardness of the bearings *B* and *C* is much lower and non-uniform. This is in accordance with the observations of the microstructure under LM.

Table 3: Hardness measurements of the sintered bearings.
Tabela 3: Trdota izmerjena na metalografskih obrusih sintranih ležajev

Sample designation	Measuring place	HV_1 /MPa
Bearing *A*	perpendicular	79.7
	parallel	69.1
Bearing *B*	perpendicular	46.3
	parallel	40.5
Bearing *C*	perpendicular	36.3
	parallel	50.4

Scanning electron microscopy and mapping micro-analyses (SEM/EDXS) were performed at different locations of the investigated bearings, as shown in **Figures 14 and 15**. In all cases Cu and Sn are mainly present. However, in bearings *B* and *C*, Zn is also

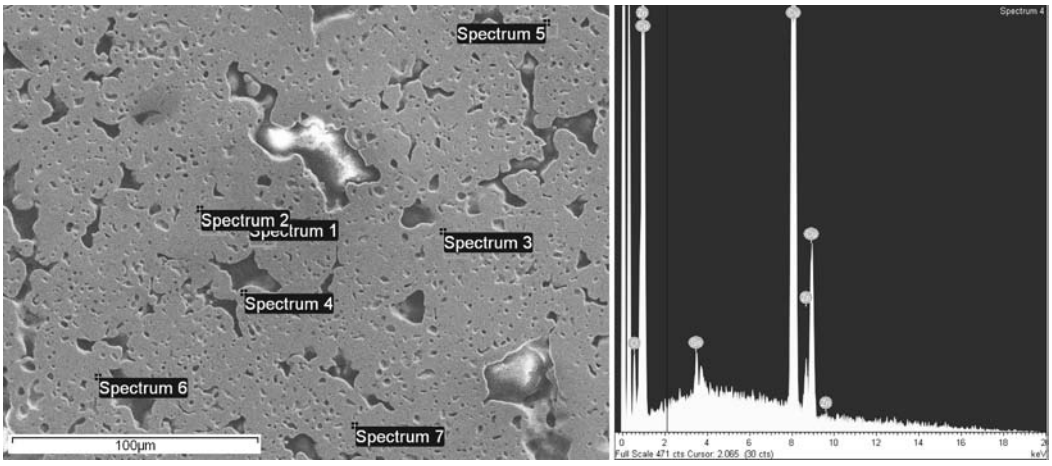

Figure 14: SEI image of the analysed surface of bearing sample *B* with designated regions where the microchemical analyses were made (a); and the corresponding characteristic EDXS spectrum 4 with visible peaks for Cu, Sn, O in Zn (b).
Slika 14: SEI-posnetek analizirane površine ležaja *B* z označenimi mesti, kjer je bila opravljena ploskovna mikrokemijska EDXS-analiza (a) in pripadajoč karakterističen EDXS-spekter 4 z vidnimi vrhovi za Cu, Sn, O in Zn (b)

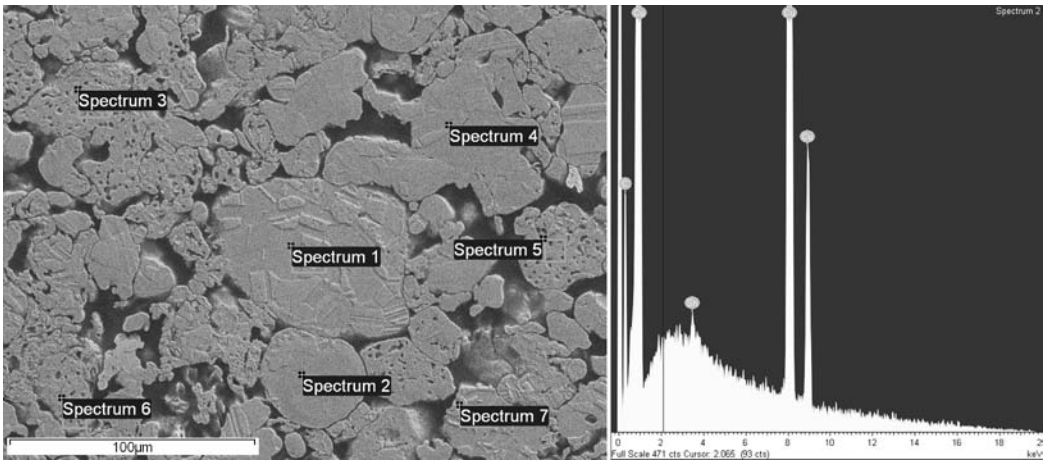

Figure 15: SEI image of the analysed surface of bearing sample *C* with designated regions where microchemical analyses were made (a); and the corresponding characteristic EDXS spectrum 2 with visible peaks for Cu, Sn, O (b)
Slika 15: SEI-posnetek analizirane površine ležaja *C* z označenimi mesti, kjer je bila opravljena ploskovna EDXS-mikrokemijska analiza (a) in pripadajoč karakterističen EDXS-spekter 2 z vidnimi vrhovi za Cu in O ter manjšim vrhom Sn (b)

present. The SEM/EDXS analyses of bearing *A* showed its relatively uniform chemical composition. The local concentration of Sn in the individual particles varied between mass fractions 8.4 % to 11.4 %. It was concluded that all the particles have practically the selected bronze bearing-alloy composition. The assessed content of oxygen is approx. 0.5 %.

The bearing *B* has a local content of Sn between mass fractions 8.3 % and 12.7 %. At one location there was a particle also containing Zn (3.6 %) and a small content of Sn (1.9 %). Obviously, powder particles of brass are also present in the powder mixtures used. Bearing *C* has the lowest local content of Sn (between 6.1 % and 11.6 %). At two locations, particles of practically pure Cu are found. This confirms that a mixture of elemental powders was used. Particles containing Zn were not found, although a bulk chemical analysis established its presence. Obviously, also in this case powder particles of brass are present in the powder mixtures. Bearings *B* and *C* also have a higher oxygen content compared to the bearings *A*. The assessed oxygen content of the bearing *B* is between 0.6 % and 2.0 % and that of bearing *C* is between 0.7 % and 1.2 %. This indicates that a poorer sintering atmosphere was used, compared to the sintering atmosphere used for bearings *A*.

4 CONCLUSIONS

This work presents an excellent example of how the selected raw materials and process conditions can drastically influence the final functional properties of a sintered product. The results of our analyses and investigations showed that all the investigated bearings have a similar average chemical composition (bronze of type Cu-10 % Sn). However, they significantly differ in terms of the microstructure and consequently also in the mechanical and functional properties. This is first of all due to the different raw materials being used. It can be supposed that for the production of bearing *A* a chemically homogeneous Cu-Sn10 % atomized alloyed powder is used, while for the production of bearings *B* and *C* powder mixtures of elemental Cu and Sn are used. In this case, less pure raw materials are also used with some presence of Zn and Pb. In the case of bearing *A* also much better conditions of compaction and the sintering process were used. The density of bearing *A* is more uniform and the interconnected porosity enables optimal oil filling. These bearings exhibit no presence of secondary intermetallic phases, oxides and other inclusions. The average hardness of the bearings *A* is much higher and uniform. All these facts explain why these bearings have much better functional properties in comparison with the bearings *B* and *C*.

5 REFERENCES

[1] P/M-Encyclopedia; CD-ROM; European Powder Metallurgy Association, 2001

[2] Sint - Prüfnormen (SPN); Sintermetalle; DIN 30 910, Teil 1&3, WLB, Sintermetalle für Lager und Formteile mit Gleiteigenschaften, Oktober 1990

[3] Thümmler, R. Oberacker: An Introduction to Powder Metallurgy, The Institute of Materials, The University Press, Cambridge, London, UK, 1993

[4] R. M. German: Powder Metallurgy Science, Metal Powder Industries Federation (MPIF), Princeton, New Jersey, 2nd edition, 1994

[5] E. Klar et al: Powder Metallurgy, Metals Hand Book, 9th Edition, Volume 7, P/M ASM Handbook Committee, American Society For Metals, Ohio, 1984

[6] Sintered metal materials, excluding hardmetals – Permeable sintered metal materials – Determination of density, oil content and open porosity; International standard ISO

[7] Sint - Prüfnormen (SPN); Prüfung der Sinterhärte; DIN 30 911, Teil 4, Oktober 1990

[8] Database of Thermochemical and Physical Properties (TAPP), ES Microware, Hamilton, Ohio, ZDA

[9] E. A. Brandes, G. B. Brook: Smithells metals reference Book, 7th Edition, Butterworth Heinemann, Oxford, 1992

[10] ThermoCalc; web page: http://www.thermocalc.com/